Article

Neuron

# Molecular Mechanism of AMPA Receptor Modulation by TARP/Stargazin

## Highlights

- AMPAR membrane core and C-tail are required and sufficient to enable TARP activity
- TARPs bind at the interface between adjacent AMPAR subunits
- TARP membrane domains 3 and 4 and extracellular loop 2 partake in AMPAR modulation
- TARPs primarily destabilize the closed state to promote channel opening

## Authors

Anat Ben-Yaacov, Moshe Gillor, Tomer Haham, Alon Parsai, Mohammad Qneibi, Yael Stern-Bach

## Correspondence

yaelste@ekmd.huji.ac.il

## In Brief

Combining systematic mutagenesis and electrophysiology, Ben-Yaacov et al. identified the protein-protein interfaces and mode of action enabling modulation of AMPA receptor trafficking and gating by the auxiliary TARPs, processes which are fundamental for excitatory synaptic signaling in health and disease.

Ben-Yaacov et al., 2017, Neuron *93*, 1126–1137
March 8, 2017 
http://dx.doi.org/10.1016/j.neuron.2017.01.032

CellPress

CellPress

Neuron
Article

# Molecular Mechanism of AMPA Receptor Modulation by TARP/Stargazin

Anat Ben-Yaacov,[1] Moshe Gillor,[1] Tomer Haham,[1] Alon Parsai,[1] Mohammad Qneibi,[1] and Yael Stern-Bach[1,2,*]
[1]Department of Biochemistry and Molecular Biology, Institute for Medical Research Israel-Canada (IMRIC), Faculty of Medicine, The Hebrew University of Jerusalem, Jerusalem 91120, Israel
[2]Lead Contact
*Correspondence: yaelste@ekmd.huji.ac.il
http://dx.doi.org/10.1016/j.neuron.2017.01.032

## SUMMARY

**AMPA receptors (AMPARs) mediate the majority of fast excitatory transmission in the brain and critically contribute to synaptic plasticity and pathology. AMPAR trafficking and gating are tightly controlled by auxiliary transmembrane AMPAR regulatory proteins (TARPs). Here, using systematic domain swaps with the TARP-insensitive kainate receptor GluK2, we show that AMPAR interaction with the prototypical TARP stargazin/γ2 primarily involves the AMPAR membrane domains M1 and M4 of neighboring subunits, initiated or stabilized by the AMPAR C-tail, and that these interactions are sufficient to enable full receptor modulation. Moreover, employing TARP chimeras disclosed a key role in this process also for the TARP transmembrane domains TM3 and TM4 and extracellular loop 2. Mechanistically, our data support a two-step action in which binding of TARP to the AMPAR membrane domains destabilizes the channel closed state, thereby enabling an efficient opening upon agonist binding, which then stabilizes the open state via subsequent interactions.**

## INTRODUCTION

Synaptic plasticity denotes the ability of neurons to dynamically modulate pre-existing synaptic connections and is a process suggested to play a fundamental role in learning and memory. The AMPA-type glutamate receptors (AMPARs) mediate the majority of fast excitatory transmission and critically contribute to synaptic plasticity as well as to several neurodegenerative and neuropsychiatric disorders (Palmer et al., 2005). AMPAR function at the synapse depends not only on the identity and composition of the pore-forming subunits (GluA1-4) (Hollmann and Heinemann, 1994; Seeburg, 1993) but also on the interaction with various accessory proteins (Jackson and Nicoll, 2011; Schwenk et al., 2012; Tomita, 2010). Of these, the transmembrane AMPAR regulatory proteins (TARPs) were shown to be essential auxiliary subunits for native AMPAR (Chen et al., 2000; Hashimoto et al., 1999), controlling both receptor trafficking and gating. In addition to promoting AMPAR surface expression and localization, data accumulating from several studies, including from our lab, showed that the prototypical TARP, γ2, also known as stargazin, functions as a positive allosteric modulator of AMPARs: γ2 slows receptor deactivation, reduces desensitization and accelerates recovery from desensitization, enhances agonist affinity and efficacy, increases channel conductance and open probability, and reduces channel block by intracellular polyamines (Priel et al., 2005; Shelley et al., 2012; Soto et al., 2007; Tomita et al., 2005; Turetsky et al., 2005). TARPs are divided into two groups, of which type I TARPs, comprising γ2, γ3, γ4, and γ8, are all positive modulators of AMPAR, while type II TARPs, consisting of γ5 and γ7, exhibit distinct and diverse effects (Cho et al., 2007; Milstein et al., 2007).

AMPARs are tetramers assembled as dimer-of-dimers (Sobolevsky et al., 2009). Each subunit contains four principal domains: two extracellular domains—the amino-terminus (NT), primarily directing receptor assembly, and the S1-S2 ligand-binding domain (LBD); a membrane-embedded channel domain, composed of three transmembrane domains (M1, M3, and M4) and a re-entered loop (M2); and an intracellular C-tail (CT), implicated mainly in trafficking (Traynelis et al., 2010). TARPs contain four transmembrane domains (TM1–TM4), with intracellular amino-terminal domain (NTD) and carboxy-terminal domain (CTD), and two extracellular loops (EX1 and EX2) (Osten and Stern-Bach, 2006). Over the years, several studies implicated the AMPAR membrane domains and the LBD in receptor modulation by TARPs. The membrane domains were suggested to mainly associate with modulation of channel conductance and polyamine block, and the LBD and linkers connected to the channel were implicated in the control of receptor kinetics and pharmacology (Dawe et al., 2016; MacLean et al., 2014; Terhag et al., 2010; Tomita et al., 2006). Indeed, contact points for γ2 have been located in critical sites in these domains and even in the NT (Cais et al., 2014). In TARPs, roles for the large extracellular loop EX1 and the CTD have been identified, with EX1 main involvement in the regulation of AMPAR biophysical properties, and the CTD in the modulation of trafficking (Tomita et al., 2005; Turetsky et al., 2005), although later studies implicated the CTD, as well as other intracellular parts, in the modulation of the biophysical properties as well (Milstein and Nicoll, 2009; Soto et al., 2014). Nonetheless, a comprehensive understanding of the sequence and role of these interactions in AMPAR modulation by TARPs is still lacking.

Here, we employed systematic domain swaps between AMPAR and the TARP-insensitive kainate receptor GluK2

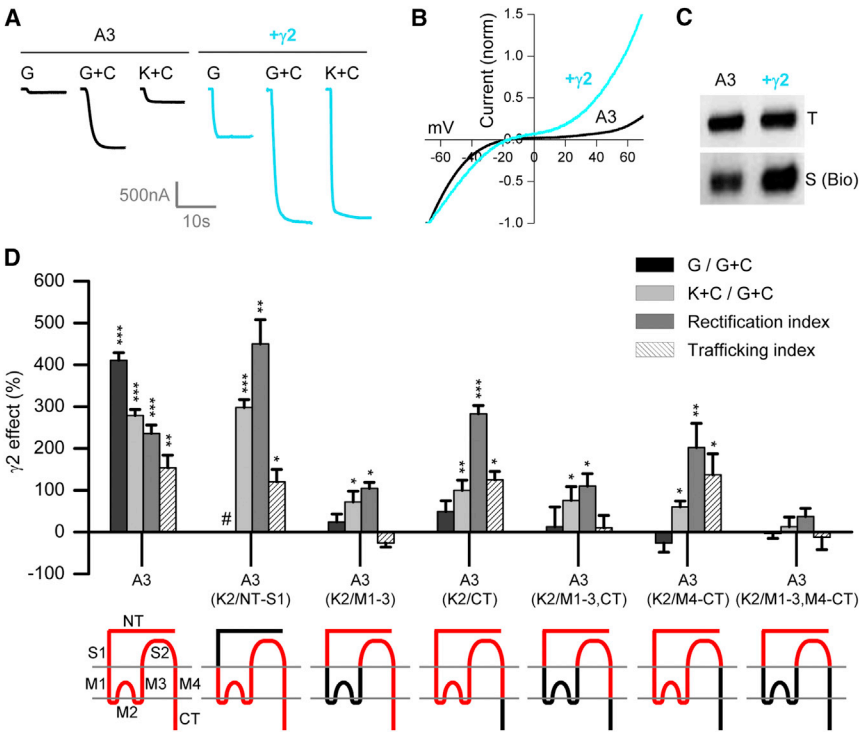


**Figure 1. Modulation of GluA3 Chimeras by TARP γ2**

(A) Representative TEVC recordings from oocytes expressing GluA3 without (black traces) or with γ2 (blue traces) in response to 10 s application of 1 mM glutamate in the absence (G) and presence of 0.1 mM cyclothiazide (G+C) and to 0.1 mM kainate with cyclothiazide (K+C).

(B) A representative current-voltage plot obtained in response to 1 mM glutamate with 0.1 mM cyclothiazide in oocytes expressing GluA3 with and without γ2 as indicated. Currents were normalized to the value recorded at −70 mV.

(C) Surface biotinylation assay performed on oocytes expressing GluA3 with and without γ2 as indicated. Shown are representative blots (n = 3) of total (T) and surface (S) biotinylated protein fractions exposed to anti-GluA3 antibodies.

(D) Summary of γ2 percent effects on gating and trafficking of GluA3 and GluA3/GluK2 chimeras, deduced from the experiments shown in (A)–(C). As explained in the main text, black bars (G/G+C) denote the γ2 effect on receptor desensitization; light gray bars (K+C/G+C) signify the change in kainate efficacy; gray bars (rectification index) depict the impact on intracellular polyamine block; and stripped bars (trafficking index) correspond to changes in receptor protein surface delivery. Bars represent mean ± SEM; see also Table S1 for details. Significance (+γ2): *<0.05; **<0.01; ***<0.001. Chimera A3(K2/NT-S1) exhibits a self-inherited desensitization block (#). Cartoons depict receptor subunit topology in which GluA3 domains are colored in red and the corresponding GluK2 domain substitutions in black.

(Chen et al., 2003) and performed functional and biochemical analysis to identify the protein-protein interfaces and mode of action enabling receptor modulation by γ2. We found that the AMPAR membrane domains and the CT are necessary and sufficient to enable receptor modulation by γ2, and that γ2 is situated in between adjacent receptor subunits. Moreover, we disclosed a key role in this process for the TARP domains TM3-EX2-TM4. These results are consistent with the recently published cryo-electron microscopy (EM) structures of the AMPAR GluA2 in complex with γ2 (Twomey et al., 2016; Zhao et al., 2016). Beyond that, we provide data suggesting a two-step mechanism in which the mere binding of TARP to the AMPAR membrane domains and the CT imposes conformational changes in these domains that destabilize the channel closed state, thereby promoting a more efficient channel opening upon agonist binding. Subsequently, conformational changes induced by agonist binding may allow interactions between extracellular parts of the receptor and TARPs, which in turn, stabilize the open state (Shaikh et al., 2016; Twomey et al., 2016; Zhao et al., 2016).

## RESULTS

### Functional Screen of GluA3 Chimeras Indicated the Involvement of the AMPAR Membrane Domains and the CT in γ2 Modulation of Receptor Properties

In order to identify the domains by which γ2 modulates AMPAR properties, we first analyzed a series of GluA3 chimeras having discrete domain swaps with the kainate receptor GluK2 (Ayalon and Stern-Bach, 2001; Stern-Bach et al., 1994). We expressed these chimeras with and without γ2 in *Xenopus laevis* oocytes and used whole-cell two-electrode voltage clamp (TEVC) recordings to test the γ2 effects on receptor function, focusing on desensitization, agonist efficacy, and intracellular polyamine block, and employed membrane protein biotinylation to measure the impact of γ2 on receptor surface delivery.

First, for estimation of the γ2 effect on receptor desensitization, we measured current responses to glutamate in the absence and presence of the AMPAR desensitization blocker cyclothiazide (Figure 1A; G and G+C, respectively). Because of fast AMPAR desensitization, occurring in a few milliseconds, only a small steady-state current can be typically recorded in TEVC following application of glutamate alone (G), while the full response is uncovered in the presence of the desensitization blocker (G+C). Broadly, changes in the ratio between the current amplitudes in the absence and presence of cyclothiazide (G/G+C) can be thus used to estimate the effect of γ2 on receptor desensitization (the higher the ratio the weaker the desensitization), and changes in current amplitude per se in the presence of cyclothiazide can indicate the impact of γ2 on channel conductance and the number of receptors on the surface. As seen in Figure 1A, in oocytes expressing intact GluA3 without γ2, the current recorded in response to glutamate alone was only ~7% of that obtained with cyclothiazide (black traces, G and G+C, respectively; Table S1), while in oocytes co-expressing γ2 the ratio increased to ~36% (blue traces, G and G+C, respectively; Table S1), presenting on average an ~400% change (G/G+C; Figure 1D, black bar), a result consistent with the γ2 reduction of receptor desensitization. There

was also an ~2-fold increase by γ2 in the total response to glutamate in the presence of cyclothiazide (Figure 1A, G+C, black and blue traces, respectively; Table S1), consistent with an increase in channel conductance and/or surface expression; however, since the magnitude of the change highly depended on the level of receptor expression (Priel et al., 2005), we did not use this parameter in the phenotypic screen of the GluA3 chimeras.

Second, for estimation of the γ2 effect on agonist efficacy, we measured responses to saturating concentrations of the partial agonist kainate. These measurements were done in the presence of cyclothiazide (Figure 1A, K+C) to eliminate γ2 effects on receptor desensitization. As seen in Figure 1A, in oocytes expressing intact GluA3 without γ2, the response to kainate was only ~20% of the response to glutamate (black traces, K+C and G+C, respectively; Table S1), while in oocytes co-injected with γ2, the response to kainate reached almost the same amplitude of that induced by glutamate (~95%, blue traces K+C and G+C, respectively; Table S1), presenting on average an ~300% increase in the efficacy of kainate (Figure 1D, K+C/G+C, light gray bar).

Third, to measure the γ2 effect on intracellular polyamine block, we obtained current/voltage curves in response to glutamate in the presence of cyclothiazide (Figure 1B) and calculated the change in current rectification index (experimental procedures), which presented on average an increase of ~250% for intact GluA3 (Figure 1D, dark gray bar; Table S1). Finally, we used a membrane protein biotinylation assay to determine the γ2 effect on receptor surface delivery (Figure 1C). To correct for differences in total protein expression, we calculated the effect of γ2 on the ratio of surface (S) biotinylated to total (T) receptor protein expression, demonstrating an ~150% increase in surface expression for intact GluA3 (Figure 1D, trafficking index, striped bar; Table S1). Overall, the effects of γ2 on intact GluA3 were similar to those reported for AMPAR GluA2 or GluA1 (Kott et al., 2009; Priel et al., 2005; Soto et al., 2007; Tomita et al., 2005).

The above tests were performed on various GluA3 chimeras having discrete domain substitutions with GluK2. Current responses to glutamate of all chimeras were similarly enhanced by cyclothiazide (Table S1), except for chimera A3(K2/NT-S1), having the GluK2 extracellular domains NT and S1, which does not desensitize in response to glutamate (Stern-Bach et al., 1998). In addition, all chimeras contained the flip isoform, which enables a complete desensitization block by cyclothiazide; thus, in addition to using saturated concentrations of cyclothiazide and agonists, the reported modulatory effects of γ2 on the efficiency of cyclothiazide (Tomita et al., 2006) were minimized or eliminated. As shown in Figure 1D, chimera A3(K2/NT-S1) basically retained the modulation by γ2 on kainate efficacy, current rectification, and surface delivery (effect on receptor desensitization could not be evaluated due to the non-desensitizing phenotype of the chimera). The apparent increase in the rectification index observed with this chimera was not statistically different from the γ2 effect on intact GluA3. In contrast, γ2 effects were significantly impaired in chimeras containing exchanges of the membrane domains and/or the CT. First, exchange of either the membrane domains M1-M2-M3 (M1-3) or the CT abolished the γ2 effect on receptor desensitization (Figure 1D, black bars, chimeras A3[K2/M1-3] and A3[K2/CT], respectively). Second, γ2 effect on kainate efficacy was also significantly impaired in those chimeras compared to intact GluA3 ($p < 0.01$), although not completely abolished, and a similar phenotype was exhibited by chimera A3(K2/M1-3,CT), containing the co-exchange of these domains (Figure 1D, light gray bars). Modulation of kainate efficacy by γ2 was also still apparent in chimera A3(K2/M4-CT), containing the exchange of the CT with the membrane domain M4 but totally lost in chimera A3(K2/M1-3,M4-CT), having exchange of the entire membrane core and the CT. γ2 effect on current rectification was significantly impaired by the M1-3 exchange, but not by the CT or by its co-replacement with M4, and abolished only when the entire membrane core and the CT were co-replaced (Figure 1D, dark gray bars). Precise kinetic measurements by fast perfusion patch-clamp technology could not be performed on the chimeras having partial exchanges of the membrane domains or the CT because of very low expression (Table S1) (Ayalon and Stern-Bach, 2001). In contrast, chimera A3(K2/M1-3,M4-CT), having all membrane domains of GluK2, produced sufficient current expression for such an analysis, and, consistent with the TEVC recordings, γ2 had no effect on receptor kinetics in outside-out patches of HEK293 cells expressing this chimera: the desensitization time constants in response to 10 mM glutamate applied for 500 ms were 5.3 ± 0.2 ms and 5.4 ± 0.2 ms without and with γ2, respectively (n = 10), and the deactivation time constants in response to 1 ms application of glutamate were 2.5 ± 0.1 ms and 2.4 ± 0.2 ms without and with γ2, respectively (n = 7). Finally, γ2 enhancement of receptor surface delivery was attenuated in chimeras containing the M1-3 exchange, but not in those having only the CT replacement or the CT with M4 (Figure 1D, striped bars; Table S1). Overall, these results highlight the necessity of the membrane domains and the CT for receptor modulation by γ2.

## Functional Screen of GluK2 Chimeras Disclosed the AMPAR M1-3 and the CT as the Minimal Domains Necessary and Sufficient to Enable Modulation of GluK2 Properties by γ2

To further establish the contribution of the AMPAR membrane domains and the CT in receptor modulation by γ2, we tested reciprocal GluK2 chimeras having GluA3 exchanges of these domains (Ayalon and Stern-Bach, 2001), looking for a gain of γ2 effect. As above, we first expressed these chimeras in oocytes and used TEVC to measure responses to glutamate before and after treatment with the kainate receptor desensitization blocker Concanavalin A (Figure 2A; G and G+Co, respectively). Co-expression with γ2 had no effect on current responses of GluK2 chimeras having GluA3 replacement of either M1-3 or the CT (data not shown), presenting a phenotype no different than intact GluK2 (Figure 2A, upper traces and left bars). In contrast, current responses of chimera K2(A3/M1-3,CT), having both exchanges, were significantly increased by γ2 (Figure 2A, lower traces and right bars). Current responses to glutamate alone were increased by ~9-fold, indicating a significant reduction in receptor desensitization, coupled to an additional positive effect on channel conductance and/or surface expression as disclosed by the ~1.7-fold increase in current response after

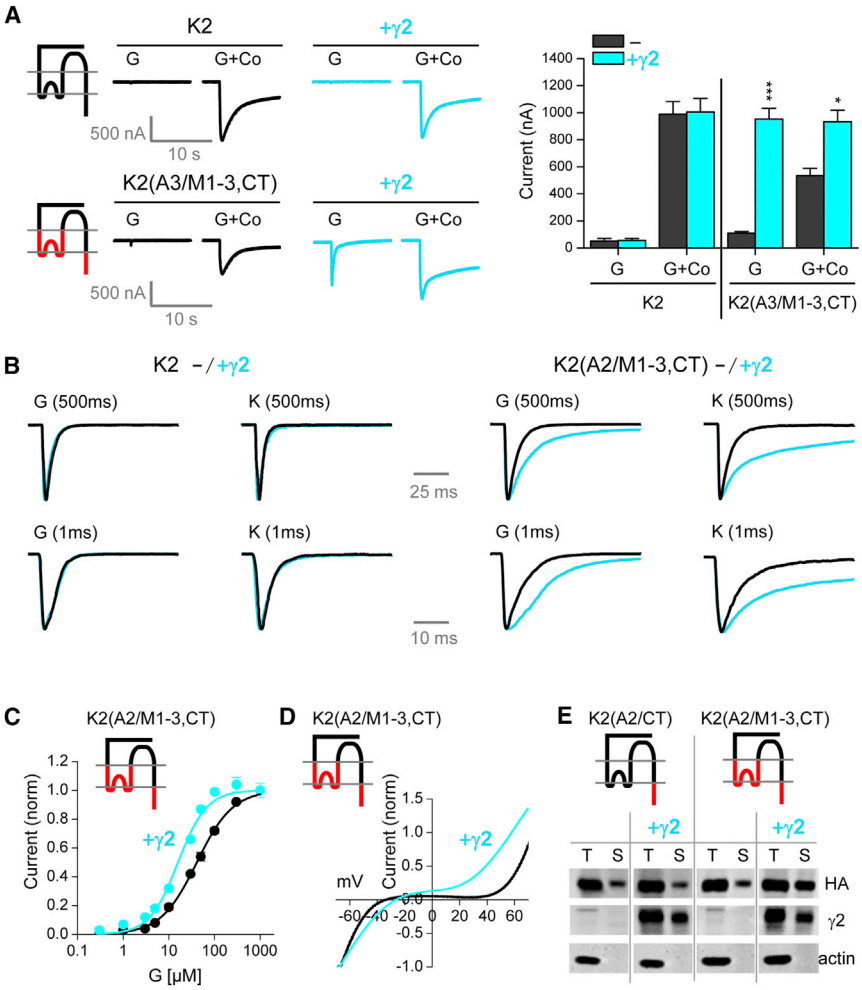


**Figure 2. Modulation of GluK2 Chimeras by γ2**

(A) Representative TEVC current traces (left) obtained from oocytes expressing intact GluK2 (upper) and chimera K2(A3/M1-3,CT) (bottom) without (black) and with γ2 (blue), in response to 1mM glutamate before (G) and after treatment with Concanavaline A (G+Co). Cartoons depict the subunit topology in which GluK2 domains are shown in black and the corresponding GluA3 domain substitutions in red. Summary of current responses (mean ± SEM, n ≥ 20) are presented on the right. Significance (+γ2): *<0.05; ***<0.001.

(B) Normalized representative traces from outside-out patches of HEK293 cells expressing GluK2 (left) or chimera K2(A2/M1-3,CT) without (black) or with γ2 (blue) in response to 3 mM glutamate (G) or 1 mM kainate (K) applied for 500 ms (top) or 1 ms (bottom) to measure receptor desensitization and deactivation, respectively (n ≥ 10).

(C) Dose-response measurements to glutamate on oocytes treated with Concanavaline A expressing chimera K2(A2/M1-3,CT) without (black) and with γ2 (blue). Responses to increasing concentrations of glutamate were normalized to the value obtained with 1 mM glutamate. Points represent mean ± SEM (n = 7). $EC_{50}$ values, deduced from individual curves, were 35.4 ± 1.3 μM and 15.0 ± 0.5 μM without and with γ2, respectively.

(D) Representative current-voltage plots (n = 7) obtained from oocytes expressing chimera K2(A2/M1-3,CT) without (black) and with γ2 (blue) in response to 1 mM glutamate (after Concanavaline A treatment). Currents were normalized to the value recorded at −70 mV.

(E) Surface biotinylation assays performed on HEK293 cells expressing chimeras K2(A2/CT) and K2(A2/M1-3,CT) with and without γ2. Shown are representative blots (n = 5) of the total (T) and surface (S) biotinylated protein fractions of the chimeras and γ2 detected by exposure to anti-HA and anti-γ2 antibodies, respectively. Exposure to anti-actin antibodies served as control for cell membrane integrity.

the treatment with Concanavalin A. Similar observations were obtained for GluK2 chimeras having M1-3 and CT exchanges with the other AMPAR subunits GluA2 and GluA1 (data not shown). To note, GluK2 chimeras having only the M1 or M2 substitutions were not functional (Ayalon and Stern-Bach, 2001), thus preventing us from examining the relative contribution of each of these domains to modulation by γ2.

Next, encouraged by the positive results, we performed fast perfusion outside-out patch clamp recordings in HEK293 cells, focusing on the chimeras containing the GluA2 exchanges because they expressed better than those having the GluA3 or GluA1 substitutions. Similar to intact GluK2, application of glutamate or kainate for 500 ms to patches expressing chimera K2(A2/M1-3,CT) without γ2 induced fast and almost complete desensitizing responses to both agonists, though slightly slower (Figure 2B, upper black traces; Table S2). However, while co-expression with γ2 had no effect on current responses of intact GluK2, it significantly slowed the current decay of K2(A2/M1-3,CT) in response to both agonists, reaching a significant elevated steady state, which was more pronounced for the response to kainate (Figure 2B, upper blue traces; Table S2). Co-expression with γ2 also slowed the deactivation kinetics of K2(A2/M1-3,CT) in response to a brief 1 ms pulse of glutamate or kainate, but not of intact GluK2 (Figure 2B, lower traces; Table S2). Moreover, although kainate induced fast desensitizing responses in GluK2 and the chimera, peak current, in both cases, reached only ~50% of that produced by glutamate when recorded on the same patch (Table S2; K/G current ratio), consistent with kainate being a partial agonist on GluK2 and the chimera. Compatible with its effect on AMPAR, γ2 increased the efficacy of kainate on K2(A2/M1-3,CT), reaching ~70% of the glutamate-evoked amplitude, but had no effect on intact GluK2 (Table S2). Similar observations were made on the compatible K2(A3/M1-3,CT) and K2(A1/M1-3,CT) chimeras (Table S2). The γ2 modulatory effects on receptor desensitization, deactivation, and kainate efficacy were tightly dependent on the co-exchange of M1-3 and the CT, as γ2 had no significant effect on any of these parameters when expressed with the chimeras having only the M1-3 or the CT exchange (Table S2; K2 [A2/M1-3] and K2[A2/CT], respectively).

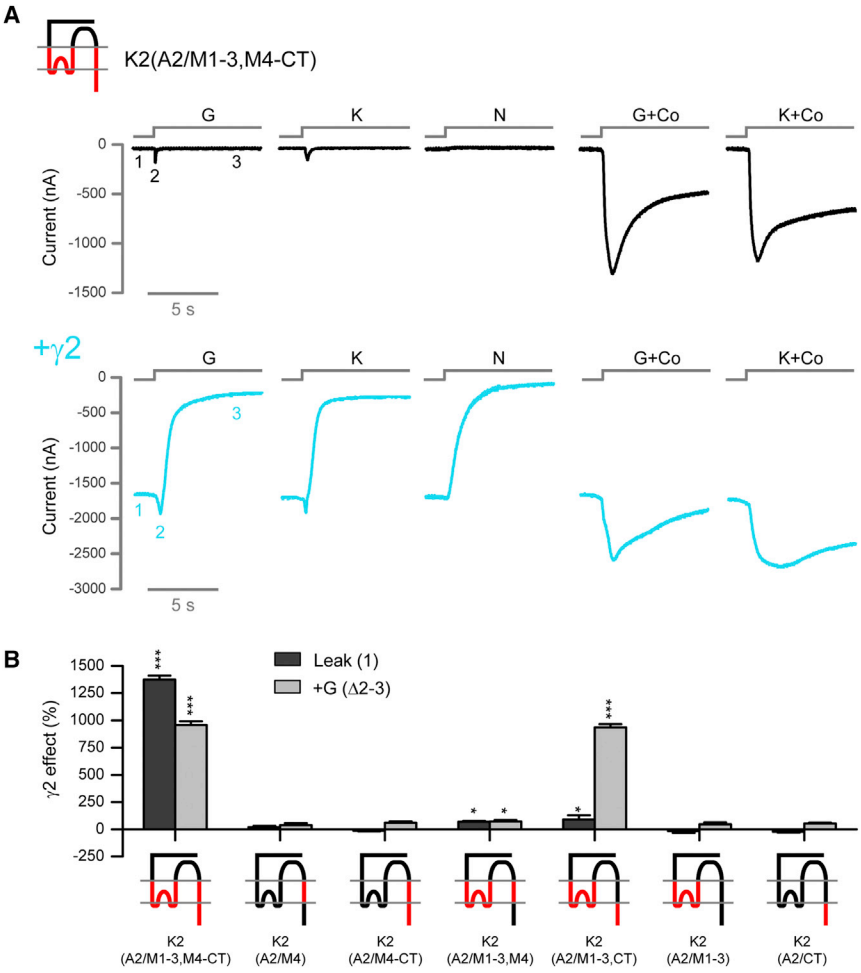


**Figure 3. Assessment of the Contribution of AMPAR M4 to Modulation by γ2**

(A) Representative TEVC current traces obtained from oocytes expressing chimera K2(A2/M1-3,M4-CT) without (top) and with γ2 (bottom) in response to 10 s application of 1 mM glutamate (G) or 0.1 mM kainate (K), before and after treatment with Concanavaline A (Co), or 0.1 mM of the open channel blocker 1-Naphthyacetyl spermine (N). Numbers on the first traces denote the basal current obtained upon clamping the oocyte (1) and that recorded after agonist application at peak (2) and after reaching a steady state (3).

(B) Summary of γ2 percent effects on basal leak current (points 1 in A) and the response to glutamate (+G, calculated as the difference between points 2 and 3 in A), of various GluK2 chimeras expressed in oocytes (red lines in the respective cartoons denote the particular GluK2 domains exchanged by GluA2). Bars represent mean ± SEM ($n \geq 50$). Significance (+γ2): *<0.05; **<0.001.

To further examine the γ2 effects on function of chimera K2(A2/M1-3,CT), we then tested its effects on receptor apparent affinity to glutamate and on intracellular polyamine block (Figures 2C and 2D). Co-expression of γ2 with K2(A2/M1-3,CT) in oocytes induced a significant leftward shift in the glutamate dose-response curve, presenting ~2-fold reduction in the $EC_{50}$ value (Figure 2C), and caused a significant change in current rectification, most prominent at positive membrane potentials (Figure 2D). These features, as well, were not affected by γ2 when co-expressed with chimeras K2(A2/M1-3) or K2(A2/CT) (data not shown). Finally, surface protein biotinylation assays conducted in HEK293 cells on these chimeras demonstrated a significant enhanced trafficking of K2(A2/M1-3,CT) when co-expressed with γ2, but not of K2(A2/CT) (Figure 2E) or K2(A2/M1-3) (data not shown). Taken together, the above results establish the AMPAR M1-3 and the CT as the domains necessary and sufficient for enabling γ2 modulation of both trafficking and gating.

## Expression of γ2 with a GluK2 Chimera Having AMPAR Exchange of the Entire Membrane Core and the CT Resulted in a Constitutively Active Channel

The results obtained from the screen with the GluA3 chimeras (Figure 1) as well as from other reports (Terhag et al., 2010) indicated that M4 may also be involved in the ability of γ2 to modulate AMPAR function. Therefore, we constructed a new GluK2 chimera, K2(A2/M1-3,M4-CT), having the exchange of all membrane domains and the CT, to test whether the inclusion of M4 would lead to an additional modulation by γ2 compared to chimera K2(A2/M1-3,CT). Surprisingly, co-expression of K2(A2/M1-3,M4-CT) with γ2 in oocytes led to a novel phenomenon where extraordinary high basal, leak currents were observed prior to glutamate application (Figure 3A, blue trace, point 1). This phenomenon was not seen in oocytes expressing the chimera alone (upper traces). The addition of glutamate led to a small inward current, followed by a significant decline (Figure 3A, blue trace, points 2 and 3, respectively), reaching a steady-state value close to the basal current obtained in oocytes expressing the chimera without γ2 (Figure 3A, black trace, point 1). This γ2-dependent abnormal phenotype is similar to the effect of the classic lurcher mutation in M3, causing a constitutive channel opening in the absence of agonists (Klein and Howe, 2004; Wollmuth et al., 2000). Similar to what was shown for the lurcher mutation, application of the open channel blocker 1-naphthyacetyl spermine to oocytes expressing the chimera with γ2 caused a complete abolishment of the leak current (Figure 3A, N), suggesting that γ2 interaction with the chimera, like the lurcher mutation, imposed a conformational change in the membrane domains causing spontaneous channel opening. This constitutive activity also indicated that the small inward current induced by glutamate (but not by 1-naphthyacetyl spermine) and its rapid decline resulted from further receptor activation followed by desensitization. Indeed, after treatment with Concanavalin A, the response to glutamate was greater than that obtained without the desensitization blocker and declined only slightly (Figure 3A, G+Co). Therefore, for the total response to glutamate

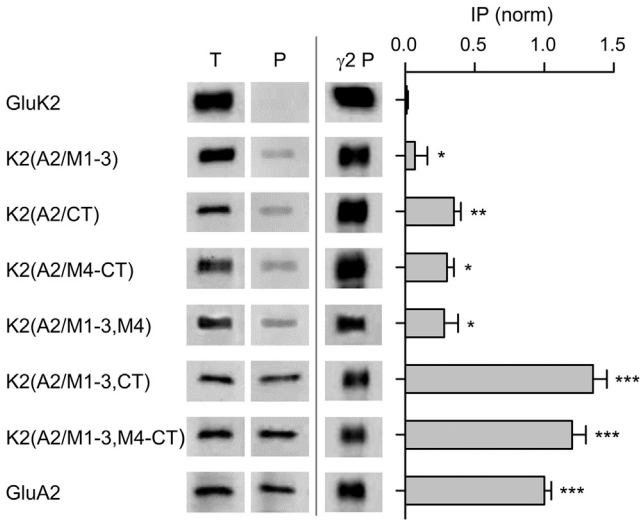


**Figure 4. Identification of AMPAR Domains Mediating the Physical Interaction with γ2**

Various GluK2 chimeras were expressed in HEK293 cells with γ2 and co-immunoprecipitated using anti-γ2 antibodies. Shown are representative blots of total (T) and precipitated (P) fractions of the chimeras (left) and γ2 (right) detected by exposure to anti-HA and anti-γ2 antibodies, respectively. Bars on the right of the blots represent mean ± SEM ($n \geq 3$) of the extent of receptor protein co-precipitated with γ2 (IP), calculated as described in STAR Methods Procedures and normalized to the value obtain for intact GluA2.

under normal conditions, we calculated the difference between peak (point 2) and steady-state (point 3) currents and used this value to estimate the γ2 effect on the agonist-induced activity (Figure 3B). Similar results were obtained for the responses to the agonist kainate before and after treatment with Concanavalin A (Figure 3A, K and K+Co, respectively). Except for promoting constitutive activity, γ2 effects on desensitization and deactivation kinetics of chimera K2(A2/M1-3,M4-CT) were similar to those observed for K2(A2/M1-3,CT) lacking the M4 substitution (Table S2).

In contrast to the results obtained for the inclusion of M4 in the M1-3 and CT co-exchange, replacing only M4, or only M4 and the CT, enabled neither modulation of GluK2 basal current by γ2 nor the response to glutamate (Figure 3B, chimeras K2[A2/M4] and K2[A2/M4-CT], respectively). A slight increase by γ2 in both basal and glutamate-induced currents was observed in the chimera having M4 co-exchanged with M1-3 (Figure 3B, chimera K2[A2/M1-3,M4]); however, no significant changes in the kinetic parameters by γ2 were observed in outside-out patch clamp recordings in HEK293 cells (Table S2). A slight increase in basal current by γ2 was also observed in chimera K2(A2/M1-3,CT) upon re-examination, but this effect was negligible compared to the robust enhancement of the response to glutamate (Figure 3B); this small increase in leak current depended, however, on the co-exchange of M1-3 and the CT, since no change in basal current was obtained in chimeras K2(A2/M1-3) and K2(A2/CT) (Figure 3B). Altogether, these results reveal a key role for M4 as well in AMPAR modulation. Mechanistically, the γ2-dependent constitutive activity also suggests that merely by binding to the AMPAR membrane domains and to the CT γ2 destabilizes the channel closed state, thereby promoting a more efficient channel opening upon agonist binding.

## Strong Physical Interaction of the Receptor with γ2 Requires the AMPAR M1-3 and the CT

The above functional screens identified the AMPAR membrane domains and the CT as crucial for receptor modulation by γ2. To determine which of these domains are the minimal domains needed for physical interaction with γ2, we expressed the various GluK2 chimeras with γ2 in HEK293 cells and conducted co-immunoprecipitation assays using antibodies against γ2. As shown in Figure 4, chimeras having the individual exchanges of M1-3 or the CT (K2[A2/M1-3] and K2[A2/CT], respectively) or in combination with M4 (K2[A2/M1-3,M4] and K2[A2/M4-CT], respectively) exhibited weak to moderate co-precipitation with γ2. In contrast, the co-exchange of M1-3 and the CT (chimera K2[A2/M1-M3,CT]) resulted in a strong co-precipitation, to the extent obtained with GluA2, and the inclusion of M4 in the exchanged domains (chimera K2[A2/M1-3,M4-CT]) had no further effect (Figure 4). These results show that the AMPAR M1-3 and the CT together constitute the domains necessary and sufficient for full physical interaction with γ2.

## Functional Analysis of Various Pairs of GluK2 Chimeras Co-expressed with γ2 Suggested that γ2 Binds in between AMPAR Subunits

The AMPAR membrane core adopts a 4-fold structural symmetry, in which the M3 helices of the four subunits line the inside of the ion channel with the pore-forming M2 segments located at the base, while the M1 and M4 helices form the exterior part with the M1 segment of one subunit positioned closed to M4 of the adjacent subunit (Figure 7C) (Sobolevsky et al., 2009). Given this arrangement, it is plausible to hypothesize that M1 and M4, rather than M3, could serve as the main membrane domains involved in AMPAR interaction with γ2. Additionally, while M3 is almost identical in all ionotropic glutamate receptors, there are considerable differences between the receptor subtypes in the amino-acids sequence of M1 and M4 (Figure 7A), which can account for the specific interaction of γ2 with AMPARs. The CT, which emerges from M4 and whose structure is yet unknown, also exhibits high sequence diversity (Figure 7A), which can additionally contribute to the specific interaction with γ2.

The particular structural arrangement of M1 and M4 around the pore provides two possible binding sites for γ2: one between M1 and M4 within the same AMPAR subunit in the tetramer, and the other between M1 and M4 of neighboring subunits. To distinguish between these two possibilities, we took advantage of the robust effects of γ2 on leak and glutamate-induced currents of chimera K2(A2/M1-3,M4-CT) and its lack of effect on chimeras K2(A2/M1-3) and K2(A2/M4-CT) (Figures 3B and 5A, left controls) and tested whether the combined expression of the two insensitive chimeras would enable modulation by γ2. If γ2 binds to M1 and M4 within the same subunit, no change in activity by γ2 would be expected. However, if γ2 binds between M1 and M4 of neighboring subunits, one or two binding sites for γ2 would be generated in the heteromeric assemblies (Figure 5A, right cartoons), leading to possible modulation by γ2. As shown in Figure 5A (co-expression), a significant leak current was observed

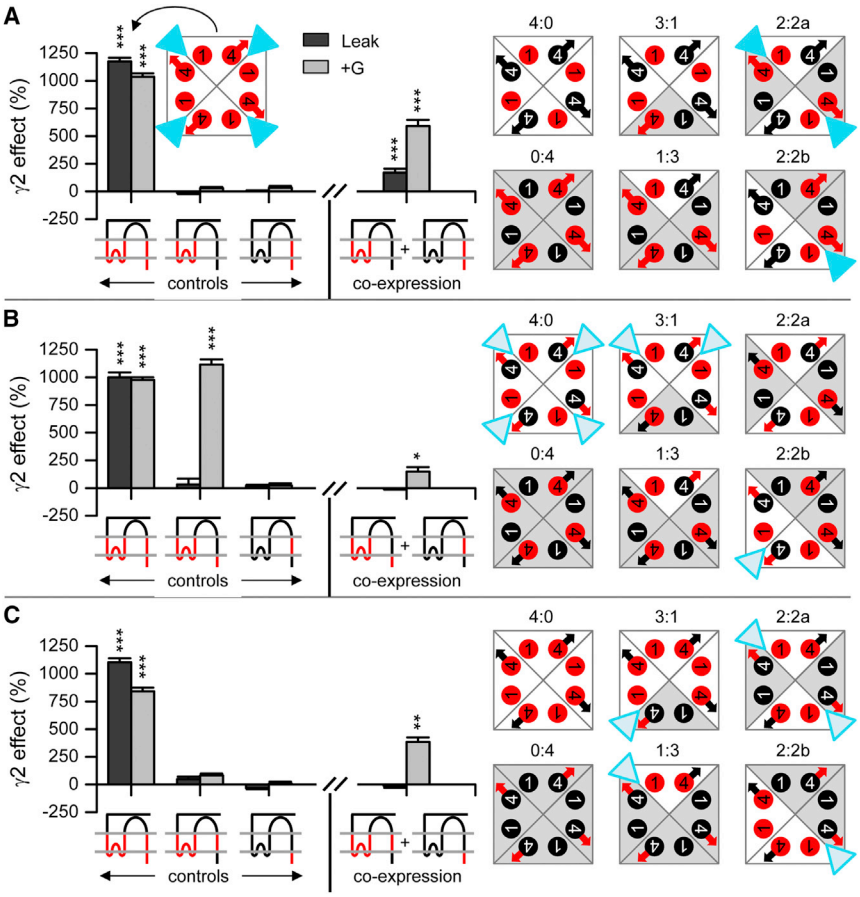


**Figure 5. Assessment of the Spatial Interaction of γ2 with AMPAR Subunits**

(A–C) γ2 effects on basal (leak) and glutamate-induced (+G) currents obtained for different pairs of GluK2 chimeras expressed in oocytes, individually (control section) or combined (co-expression section). Schematic drawings of the particular chimeras, with the corresponding domain swaps (black-GluK2, red-GluA2), are depicted underneath the panels. Chimera K2(A2/M1-3,M4-CT) served as a reference for the co-expressions (control section, first bars). Bars represent mean ± SEM (n ≥ 25). Significance (+γ2): *<0.05; **<0.01; ***<0.001. Cartoons show the tetrameric organization of M1 and M4 (circles) and the CT (arrows) of each of the four receptor subunits. Shown are the various homomeric and heteromeric assemblies resulting from the particular co-expressed chimeras, where the GluA2 and GluK2 domains are colored in red and black, respectively. To distinguish the two co-expressed subunits in the different assemblies, the quadrants corresponding to one of the chimeras are shaded light gray. Assuming equal protein expression and random assembly, the probability of each configuration to occur is: 4:0 and 0:4, 6.25% each; 3:1 and 1:3, 25% each; 2:2a, 12.5%; and 2:2b, 25%. The γ2 (triangle) is placed on the various assemblies at the putative binding sites formed by the AMPAR M1 and M4-CT (blue) or M1 and the CT (light blue) of adjacent subunits.

in oocytes expressing γ2 and the two chimeras as well as an enhanced response to glutamate, a result supporting an inter-subunit binding mode for γ2. The observed γ2 effects on leak and glutamate-induced currents were significantly weaker than the impact of γ2 on chimera K2(A2/M1-3,M4-CT) (Figure 5A, controls). However, this is expected based on the observation that the magnitude of the γ2 effect on AMPAR function depends on the number of γ2 molecules associated with the receptor (Kim et al., 2010; Milstein et al., 2007); while chimera K2(A2/M1-3,M4-CT) contains four putative binding sites (Figure 5A, left cartoon), only zero, one, or two sites are generated in the heteromeric assemblies, with the majority having only one binding site (Figure 5A, right cartoons).

The induction of the high leak current by γ2 in chimera K2(A2/M1-3,M4-CT) required not only the co-exchange of M4 with M1-3 but also the CT (Figure 3B); therefore, given the potential structural flexibility of the CT (Choi et al., 2013; Sobolevsky et al., 2009), we asked whether its specific positioning relative to M1 and M4 is important. To answer this question, we tested the expression of two additional pairs of GluK2 chimeras: (1) K2(A2/M1-3,CT) with K2(A2/M4), in which the AMPAR M1-3 and the CT are contributed by one subunit in heteromeric assemblies and the M4 by the neighboring subunit (Figure 5B), and (2) K2(A2/M1-3,M4) with K2(A2/CT), forming heteromers in which the AMPAR M1-3 and M4 reside in the same subunit and the CT on the adjacent one (Figure 5C). In both cases, no change in basal current by γ2 was observed in oocytes expressing the paired chimeras (Figures 5B and 5C, co-expression, black bars), while an apparent increase in the response to glutamate was obtained (Figures 5B and 5C, co-expression, gray bars). These results indicated that (1) for the induction of leak current (spontaneous activity) the CT must be linked to M4 mediating the interaction with γ2 and (2) for modulation of the glutamate-induced response it is enough for γ2 to interact with M1-3 and the CT of neighboring subunits (Figures 5B and 5C, cartoons). Again, in both experiments, the relative low magnitude of the γ2 effect can be explained by availability of only one or two binding sites for γ2 in the heteromeric assemblies (Figures 5B and 5C, cartoons). Overall, the above results strongly support an inter-subunit binding mode for γ2, in between M1 and M4-CT of neighboring subunits.

## Differential Modulation of Chimera K2(A2/M1-3,M4-CT) by γ2 and γ8 and Use of Reciprocal γ2/γ8 Chimeras Revealed the Involvement of TARP Domains TM3-EX2-TM4 in the Interaction with AMPAR

Finally, we sought to determine whether the γ2 effects on leak (spontaneous activity) and glutamate-induced currents of chimera K2(A2/M1-M3,M4-CT) are unique to γ2 or shared by the other type I TARPs, which, like γ2, are positive modulators

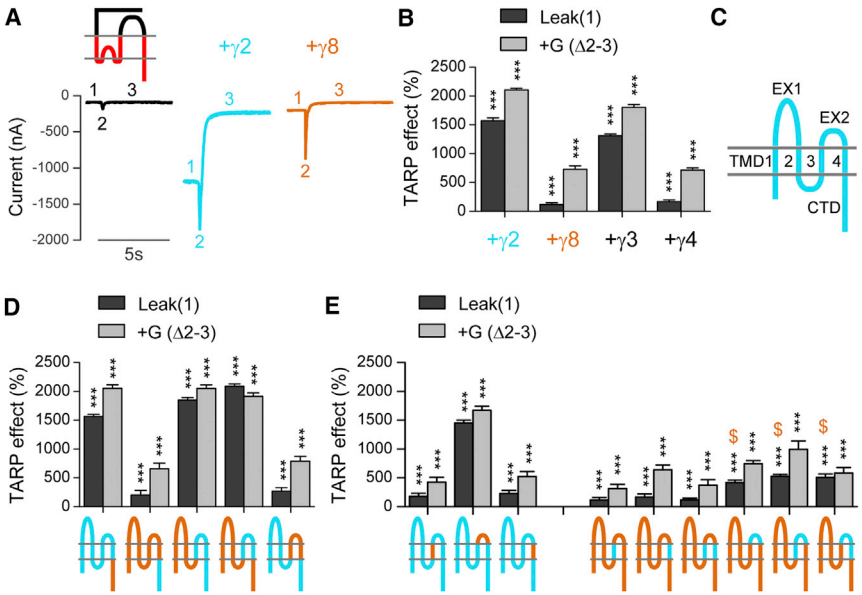


**Figure 6. TARPs Type Ia and Type Ib Differentially Modulate Properties of Chimera K2(A2/M1-3,M4-CT)**

(A) Representative traces of TEVC recordings from oocytes expressing chimera K2(A2/M1-3,M4-CT) without (black) and with γ2 (blue) or γ8 (orange), respectively. Numbers on the traces correspond to the basal current recorded upon clamping the oocyte (1) and the current response to 1mM application of glutamate at peak (2) and after reaching a steady state (3) as shown in Figure 3.

(B) Percent change in basal (leak) and glutamate-induced (+G) currents, mediated by TARP γ2, γ8, γ3, or γ4 on chimera K2(A2/M1-3,M4-CT). Bars represent mean ± SEM (n ≥ 25). Significance (+TARP): ***<0.001.

(C) Schematic drawing of TARP topology, depicting the transmembrane domains TMD1–TMD4, extracellular loops EX1 and EX2, and the CTD.

(D and E) Percent change in basal (leak) and glutamate-induced (+G) currents, mediated by various TARP chimeras, having reciprocal domain swaps between γ2 and γ8, on chimera K2(A2/M1-3,M4-CT). Bars represent mean ± SEM (n ≥ 15). Significance (+TARP chimeras): ***<0.01. Organ $ signs above bars in E denote significant differences ($p < 0.01$) from the effect mediate by intact γ8 on leak current.

of AMPAR. As shown in Figure 6A, co-expression of chimera K2(A2/M1-3,M4-CT) with γ8, the predominant TARP in the hippocampus (Tomita et al., 2003), also led to an appearance of a leak current and to an increased response to glutamate (Figure 6A, orange traces, points 1 and 2–3, respectively). Surprisingly, however, the magnitude of the effects was significantly lower ($p < 0.001$) than those obtained in the presence of γ2 (Figure 6B), although both TARPs were equally expressed as determined by western blot analysis (data not shown). Based on this result, we then tested co-expression of the chimera with TARPs γ3 and γ4, the former classified as a type Ia TARP with γ2, and the latter as a type Ib with γ8 (Tomita, 2010). Consistent with their TARP type I sub-division, the γ3 effects on chimera K2(A2/M1-3,M4-CT) were similar to those induced by γ2, while those of γ4 were similar to γ8 (Figure 6B).

Given the above characterized differences between type Ia and type Ib TARPs in modulation of chimera K2(A2/M1-3,M4-CT), we proceeded to locate the TARP domains responsible for this discrepancy using a series of γ2/γ8 chimeras, having reciprocal exchanges of discrete domains (Figure 6C). As seen in Figure 6D, mutual exchanges of the CTD did not lead to an exchange in phenotype between γ2 and γ8. However, exchanging the region from TM3 to the CTD in γ8 with the corresponding sequence of γ2 converted the phenotype to that of γ2. Consistent with the inert effect of the CTD exchanges, substituting only the region TM3-EX2-TM4 was enough for the conversion of the phenotype from γ8 to γ2. Likewise, the reciprocal exchange of TM3-EX2-TM4 of γ2 with the corresponding sequence of γ8 led to γ8-like receptor modulation (Figure 6D). To determine the relative contribution of the subdomains, we then constructed γ2 and γ8 reciprocal exchanges of TM3, EX2, and TM4, individually and in combination. Exchanging either TM3 or TM4 of γ2 with the corresponding sequence of γ8 induced responses similar to those produced by γ8, while the exchange of EX2 preserved the effects seen with γ2 (Figure 6E, three left γ2 chimeras). However, replacement of TM3 or TM4 of γ8 with the corresponding sequence of γ2 did not convert the phenotype to that of γ2, nor did the combined exchange of TM3 and TM4 (Figure 6E, three left γ8 chimeras). Likewise, exchange of the EX2 alone or in combination with TM3 or TM4 was not enough to impose the γ2 effects on chimera K2(A2/M1-3,M4-CT) (Figure 6E, three right γ8 chimeras). Compared to intact γ8, a slight but significant increase in the leak current was observed by the γ8 chimeras having the γ2 EX2 exchange, (Figure 6E, $), yet not to the extent obtained with intact γ2. Thus, converting the γ8 phenotype on chimera K2(A2/M1-3,M4-CT) to that of γ2 required the exchange of the entire TM3-EX2-TM4 region (Figure 6D). Altogether, in addition to the already identified EX1 domain (Tomita, 2010), these results disclose a key role also for the TARP TM3-EX2-TM4 domains in the functional interaction with AMPARs.

## DISCUSSION

Here we used a systematic analysis, employing loss- and gain-of-function chimeras, to identify domains needed for the many effects of TARPs on AMPARs. This analysis disclosed the AMPAR membrane domains M1-3 and the CT as the minimal elements necessary and sufficient for AMPAR-TARP-specific interactions and the modulation of receptor trafficking and gating, with an additional importance of AMPAR M4 in this process. In addition, functional analysis suggested that AMPAR interaction with TARPs occurs between M1 and M4-CT of adjacent receptor subunits. Reciprocally, we analyzed domains within type I

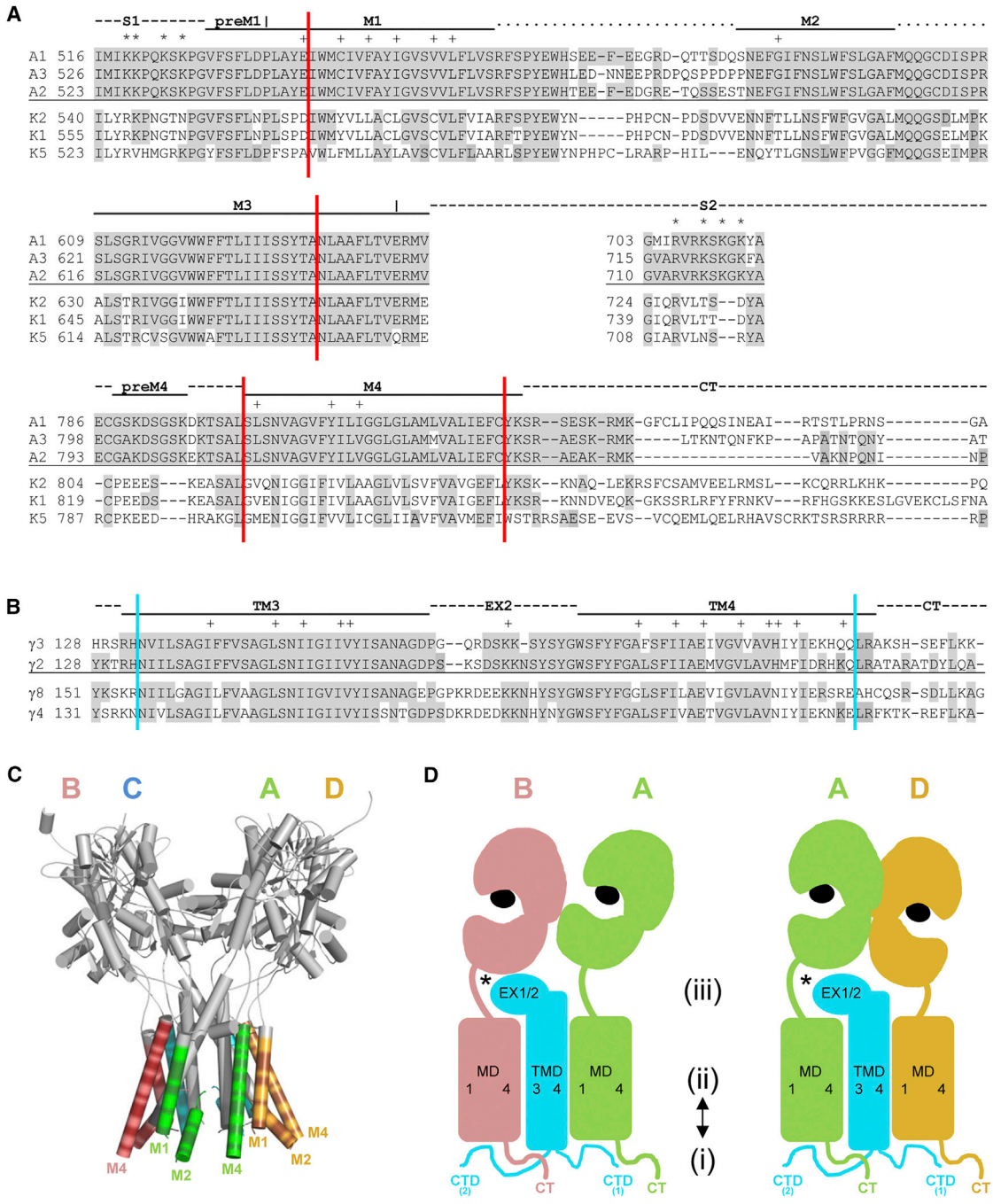


**Figure 7. Molecular Mechanism of TARP Interaction with AMPAR**

(A and B) Amino acid sequence alignment (Clone Manager software) of selective AMPA and kainate receptor subunits, and type I TARPs (numbered relative to the initiating methionine). Gray backgrounds denote residues that are identical to GluA2 or γ2, respectively. Solid and dashed lines above the sequences in (A) denote the receptor domains as depicted in the crystal structure of GluA2 (Sobolevsky et al., 2009), and dot lines mark regions not seen in structure. Lines in (B) mark the TARP domains as depicted by recent cryo-EMs (Twomey et al., 2016; Zhao et al., 2016). Plus signs (+) mark residues proposed by these structures to make contacts between GluA2 and γ2, and asterisks (*) in (A) mark positively charged residues in S1 and S2 proposed to form an electrostatic patch with γ2 in the active state. Vertical red and blue lines mark the actual boundaries of the regions exchanged in the receptor and TARP chimeras, respectively.

(C) Structure of GluA2 tetramer viewed parallel to the membrane (PDB 3KGC) generated by PyMOL software. The CT was omitted from crystallization and the NT was removed from the picture for clarification. The membrane domains M1, M2 and M4, substituted by GluA2 in the GluK2 chimeras are color coded according to the four monomers; darker colors highlight residues differing between GluA2 and GluK2. LBD and connecting linkers not exchanged by GluA2 in the γ2-positive GluK2 chimeras are in gray. M3, which has been exchanged but is almost identical between the receptor subtypes, is also colored in gray.

*(legend continued on next page)*

TARPs and identified the region containing TM3-EX2-TM4 as necessary and sufficient for imposing type Ia effects.

These results are consistent with recently published cryo-EM structures of GluA2 in complex with γ2 (Twomey et al., 2016; Zhao et al., 2016) showing γ2 positioning in between receptor subunits, with M1 of one subunit making substantial contacts with TM3 and TM4 (and possibly EX2) of γ2, and M4 of the neighboring subunit interacting with γ2 TM3. Contact points were also suggested to occur between M2 and γ2 TM4. In agreement with our analysis, the majority of the contacting residues (indicated in Figures 7A and 7B by + signs) significantly differ between AMPAR and kainate receptor subunits, thus accounting for the receptor subtype specificity toward TARPs. However, our results go further than the structural analysis by showing functional importance of these interacting interfaces, providing important and complementary insights to our understanding of the AMPAR-TARP interaction.

First, we identified a crucial role for the AMPAR CT both in physical interaction with TARP and in enabling its modulatory effects on receptor trafficking and gating. This interaction was not reported by either of the cryo-EM studies. Twomey et al. (2016) used a tandem construct in which GluA2 lacking most of its CT was fused to γ2, thereby bypassing this necessary interaction, and Zhao et al. (2016), although using a full-length GluA2, also did not detect this interaction, probably because of low structural resolution.

Second, one striking result obtained from our functional screen is the induction of TARP-dependent leak current in the GluK2 chimera having the AMPAR membrane domains and the CT (Figures 3 and 6). In the presence of TARP, this chimera exhibited high basal activity, similar to the phenotype exerted by the classic lurcher mutation in M3 (Klein and Howe, 2004; Wollmuth et al., 2000), which has been suggested to destabilize close contacts between M3 helices of the neighboring subunits forming the channel gate (Sobolevsky et al., 2009). Therefore, this TARP-dependent lurcher-like phenotype suggests that, primarily, the mere binding of γ2 to the AMPAR membrane domains imposes conformational changes in these domains that destabilize the channel closed state, thereby promoting an efficient opening of the channel upon agonist binding. These interactions may involve rearrangements of M1 and M4 to create a conformation more prone to activation. Alternatively, these interactions may destabilize the gate, through a chain of existing contacts between M1, M2, and M3 (Sobolevsky et al., 2009), or a combination of these processes. These TARP-dependent rearrangements thus affect not only properties of the channel, like conductance and polyamine block (Soto et al., 2014; Tomita et al., 2005), but also the coupling between agonist binding and channel opening, manifested by the increase in open channel probability and agonist potency (Priel et al., 2005; Tomita et al., 2005; Turetsky et al., 2005). The induction of constitutive activity in the chimera and not in wild-type AMPAR is most probably a result of a destabilized closed state in the chimera, indicated by its slight slower kinetics in the absence of γ2 compared to intact GluK2 (Table S2), which is further destabilized by the TARPs. Apart from effects on gating, we also show that TARP interaction with the AMPAR membrane domains (particularly M1-3) is important for its effects on trafficking (Figures 1 and 2).

Third, several studies emphasized the importance of interactions in the extracellular domains of TARP and AMPAR in modulation of receptor gating, primarily involving the TARP EX1 and the AMPAR LBD and connecting linkers (Dawe et al., 2016; MacLean et al., 2014; Milstein et al., 2007; Tomita et al., 2005; Turetsky et al., 2005). Indeed, the recent cryo-EM structures indicated the possible formation of electrostatic interactions between these AMPAR and TARP domains (Figures 7A and 7D, asterisks), which are proposed to stabilize the channel open state upon agonist binding, hence affecting receptor kinetics. In our screen we did not detect a role for such interactions, possibly due to the fact that the residues proposed to mediate these electrostatic interactions are mostly conserved between AMPAR and GluK2 (Figure 7A, asterisks). It is also possible that, upon agonist binding, stabilization of the active state by TARP may be achieved, not only through extracellular interactions but also through further altering interactions within the membrane domains and even the CT. Indeed, a recent study employing dynamic spectroscopy suggested that the CT and the intracellular linker between M1 and M2 move during AMPAR activation (Zachariassen et al., 2016).

Finally, our results may also provide insight into the stoichiometry of AMPAR and TARPs. Type I TARPs are subdivided into type Ia (γ2 and γ3) and type Ib (γ4 and γ8) according to their effects on AMPAR (Tomita, 2010), a segregation we also detected in our study for their effects on chimera K2(A2/M1-3,M4-CT) (Figure 6). In addition to differing effects on function, the stoichiometry of their interactions with the AMPAR was suggested to differ: up to four γ2 or γ3 proteins per receptor, but only up to two for γ4 or γ8 (Hastie et al., 2013). Our results may functionally support this stoichiometry, as effects of γ4 and γ8 on chimera K2(A2/M1-3,M4-CT) (Figure 6) were similar to effects of γ2 obtained by the co-expression of chimeras K2(A2/M1-3) and K2(A2/M4-CT), where only up to two AMPAR subunit interfaces are available for interaction with TARP (Figure 5A).

A model of AMPAR-TARP interaction and mechanism of action, incorporating our data and other recent studies (Carbone and Plested, 2016; Dawe et al., 2016; Shaikh et al., 2016; Twomey et al., 2016; Zhao et al., 2016), is illustrated in Figure 7D. Shown are two possible binding interfaces for TARP, one between AMPAR subunits A and B and the other between A and D, which are identical at the level of the membrane domain (and possibly the CT) but differing above the membrane plane where the extracellular parts of TARP (EX1/2) are positioned

(D) Cartoon model for γ2 interaction and AMPAR modulation. Shown are two AMPAR subunit interfaces formed between monomers A and B (left) and A and D (right), creating binding sites for γ2 (blue). Binding of γ2 primarily involves interactions with M1 and M4 of the neighboring subunits, initiated (i) or stabilized (ii) by interaction with the CT emerging from the particular M4. These interactions impose conformational changes enabling an efficient channel opening upon agonist binding, which in turn (iii) allow electrostatic interactions (*) between the AMPAR LBD & connecting linkers and the extracellular loops of γ2 (EX1/2) that further stabilize the open state. The orientation of γ2 CTD, implicated in AMPAR trafficking and gating, is yet unknown, thus illustrated for two options: CTD(1) or CTD(2). A similar model applies for the interfaces formed between the other equivalent subunit pairs, pair C and D and pair C and B, respectively (data not shown).

below the LBD of the subunit contributing the M4-CT region. Binding of TARP primarily involves interactions with the AMPAR M1 and M4 of the neighboring subunits, initiated (1) or stabilized (2) by interaction with the AMPAR CT. These interactions impose conformational changes in the membrane domains, enabling an efficient channel opening upon agonist binding, which in turn (3) promotes interactions between the TARP EX1/2 and the AMPAR LBD and connecting linkers, further stabilizing the open state. This two-step mechanism of action accounts for the multiple effects of TARPs on AMPAR. This mechanism may also serve as a model for the modulation of AMPAR by other auxiliary proteins, particularly cornichons, shown to work alongside to TARPs, and GSG1L, a member of the claudin superfamily, which includes the TARPs (Haering et al., 2014).

## STAR★METHODS

Detailed methods are provided in the online version of this paper and include the following:

- KEY RESOURCES TABLE
- CONTACT FOR REAGENT AND RESOURCE SHARING
- EXPERIMENTAL MODEL AND SUBJECT DETAILS
  - *Xenopus laevis* Frogs
  - Cultured Cells
- METHOD DETAILS
  - Molecular Biology
  - Heterologous Expression and Electrophysiology
  - Biochemical Assays
- QUANTIFICATION AND STATISTICAL ANALYSIS

### SUPPLEMENTAL INFORMATION

Supplemental Information includes two tables and can be found with this article at http://dx.doi.org/10.1016/j.neuron.2017.01.032.

### AUTHOR CONTRIBUTION

Conceptualization, A.B.-Y., M.G., and Y.S.-B.; Methodology, A.B.-Y., M.G., T.H., and Y.S.-B.; Investigation, A.B.-Y., M.G., T.H., A.P., and M.Q.; Writing – Original Draft, A.B.-Y., M.G., and Y.S.-B.; Writing – Review & Editing, A.B.-Y. and Y.S.-B.; Funding Acquisition, Y.S.-B.

### ACKNOWLEDGMENTS

Supported by the Israel Science Foundation (grant number 919/11). We thank A. Yaffe for technical assistance with the co-immunoprecipitation experiments and E. Isacoff and M. Ulbrich for the gift of EGFP-tagged TARPs γ3 and γ4.

Received: October 25, 2016
Revised: December 28, 2016
Accepted: January 30, 2017
Published: February 23, 2017

### REFERENCES

Ayalon, G., and Stern-Bach, Y. (2001). Functional assembly of AMPA and kainate receptors is mediated by several discrete protein-protein interactions. Neuron *31*, 103–113.

Cais, O., Herguedas, B., Krol, K., Cull-Candy, S.G., Farrant, M., and Greger, I.H. (2014). Mapping the interaction sites between AMPA receptors and TARPs reveals a role for the receptor N-terminal domain in channel gating. Cell Rep. *9*, 728–740.

Carbone, A.L., and Plested, A.J. (2016). Superactivation of AMPA receptors by auxiliary proteins. Nat. Commun. *7*, 10178.

Chen, L., Chetkovich, D.M., Petralia, R.S., Sweeney, N.T., Kawasaki, Y., Wenthold, R.J., Bredt, D.S., and Nicoll, R.A. (2000). Stargazin regulates synaptic targeting of AMPA receptors by two distinct mechanisms. Nature *408*, 936–943.

Chen, L., El-Husseini, A., Tomita, S., Bredt, D.S., and Nicoll, R.A. (2003). Stargazin differentially controls the trafficking of alpha-amino-3-hydroxyl-5-methyl-4-isoxazolepropionate and kainate receptors. Mol. Pharmacol. *64*, 703–706.

Cho, C.H., St-Gelais, F., Zhang, W., Tomita, S., and Howe, J.R. (2007). Two families of TARP isoforms that have distinct effects on the kinetic properties of AMPA receptors and synaptic currents. Neuron *55*, 890–904.

Choi, U.B., Kazi, R., Stenzoski, N., Wollmuth, L.P., Uversky, V.N., and Bowen, M.E. (2013). Modulating the intrinsic disorder in the cytoplasmic domain alters the biological activity of the N-methyl-D-aspartate-sensitive glutamate receptor. J. Biol. Chem. *288*, 22506–22515.

Dawe, G.B., Musgaard, M., Aurousseau, M.R., Nayeem, N., Green, T., Biggin, P.C., and Bowie, D. (2016). Distinct structural pathways coordinate the activation of AMPA receptor-auxiliary subunit complexes. Neuron *89*, 1264–1276.

Haering, S.C., Tapken, D., Pahl, S., and Hollmann, M. (2014). Auxiliary subunits: shepherding AMPA receptors to the plasma membrane. Membranes (Basel) *4*, 469–490.

Hashimoto, K., Fukaya, M., Qiao, X., Sakimura, K., Watanabe, M., and Kano, M. (1999). Impairment of AMPA receptor function in cerebellar granule cells of ataxic mutant mouse stargazer. J. Neurosci. *19*, 6027–6036.

Hastie, P., Ulbrich, M.H., Wang, H.L., Arant, R.J., Lau, A.G., Zhang, Z., Isacoff, E.Y., and Chen, L. (2013). AMPA receptor/TARP stoichiometry visualized by single-molecule subunit counting. Proc. Natl. Acad. Sci. USA *110*, 5163–5168.

Hollmann, M., and Heinemann, S. (1994). Cloned glutamate receptors. Annu. Rev. Neurosci. *17*, 31–108.

Jackson, A.C., and Nicoll, R.A. (2011). The expanding social network of ionotropic glutamate receptors: TARPs and other transmembrane auxiliary subunits. Neuron *70*, 178–199.

Kim, K.S., Yan, D., and Tomita, S. (2010). Assembly and stoichiometry of the AMPA receptor and transmembrane AMPA receptor regulatory protein complex. J. Neurosci. *30*, 1064–1072.

Klein, R.M., and Howe, J.R. (2004). Effects of the lurcher mutation on GluR1 desensitization and activation kinetics. J. Neurosci. *24*, 4941–4951.

Kott, S., Sager, C., Tapken, D., Werner, M., and Hollmann, M. (2009). Comparative analysis of the pharmacology of GluR1 in complex with transmembrane AMPA receptor regulatory proteins gamma2, gamma3, gamma4, and gamma8. Neuroscience *158*, 78–88.

MacLean, D.M., Ramaswamy, S.S., Du, M., Howe, J.R., and Jayaraman, V. (2014). Stargazin promotes closure of the AMPA receptor ligand-binding domain. J. Gen. Physiol. *144*, 503–512.

Milstein, A.D., and Nicoll, R.A. (2009). TARP modulation of synaptic AMPA receptor trafficking and gating depends on multiple intracellular domains. Proc. Natl. Acad. Sci. USA *106*, 11348–11351.

Milstein, A.D., Zhou, W., Karimzadegan, S., Bredt, D.S., and Nicoll, R.A. (2007). TARP subtypes differentially and dose-dependently control synaptic AMPA receptor gating. Neuron *55*, 905–918.

Osten, P., and Stern-Bach, Y. (2006). Learning from stargazin: the mouse, the phenotype and the unexpected. Curr. Opin. Neurobiol. *16*, 275–280.

Palmer, C.L., Cotton, L., and Henley, J.M. (2005). The molecular pharmacology and cell biology of alpha-amino-3-hydroxy-5-methyl-4-isoxazolepropionic acid receptors. Pharmacol. Rev. *57*, 253–277.

Priel, A., Kolleker, A., Ayalon, G., Gillor, M., Osten, P., and Stern-Bach, Y. (2005). Stargazin reduces desensitization and slows deactivation of the AMPA-type glutamate receptors. J. Neurosci. *25*, 2682–2686.

Priel, A., Selak, S., Lerma, J., and Stern-Bach, Y. (2006). Block of kainate receptor desensitization uncovers a key trafficking checkpoint. Neuron *52*, 1037–1046.

Schneider, C.A., Rasband, W.S., and Eliceiri, K.W. (2012). NIH Image to ImageJ: 25 years of image analysis. Nat. Methods *9*, 671–675.

Schwenk, J., Harmel, N., Brechet, A., Zolles, G., Berkefeld, H., Müller, C.S., Bildl, W., Baehrens, D., Hüber, B., Kulik, A., et al. (2012). High-resolution proteomics unravel architecture and molecular diversity of native AMPA receptor complexes. Neuron *74*, 621–633.

Seeburg, P.H. (1993). The TiPS/TINS lecture: the molecular biology of mammalian glutamate receptor channels. Trends Pharmacol. Sci. *14*, 297–303.

Shaikh, S.A., Dolino, D.M., Lee, G., Chatterjee, S., MacLean, D.M., Flatebo, C., Landes, C.F., and Jayaraman, V. (2016). Stargazin Modulation of AMPA Receptors. Cell Rep. *17*, 328–335.

Shelley, C., Farrant, M., and Cull-Candy, S.G. (2012). TARP-associated AMPA receptors display an increased maximum channel conductance and multiple kinetically distinct open states. J. Physiol. *590*, 5723–5738.

Sobolevsky, A.I., Rosconi, M.P., and Gouaux, E. (2009). X-ray structure, symmetry and mechanism of an AMPA-subtype glutamate receptor. Nature *462*, 745–756.

Soto, D., Coombs, I.D., Kelly, L., Farrant, M., and Cull-Candy, S.G. (2007). Stargazin attenuates intracellular polyamine block of calcium-permeable AMPA receptors. Nat. Neurosci. *10*, 1260–1267.

Soto, D., Coombs, I.D., Gratacòs-Batlle, E., Farrant, M., and Cull-Candy, S.G. (2014). Molecular mechanisms contributing to TARP regulation of channel conductance and polyamine block of calcium-permeable AMPA receptors. J. Neurosci. *34*, 11673–11683.

Stern-Bach, Y., Bettler, B., Hartley, M., Sheppard, P.O., O'Hara, P.J., and Heinemann, S.F. (1994). Agonist selectivity of glutamate receptors is specified by two domains structurally related to bacterial amino acid-binding proteins. Neuron *13*, 1345–1357.

Stern-Bach, Y., Russo, S., Neuman, M., and Rosenmund, C. (1998). A point mutation in the glutamate binding site blocks desensitization of AMPA receptors. Neuron *21*, 907–918.

Terhag, J., Gottschling, K., and Hollmann, M. (2010). The transmembrane domain C of AMPA receptors is critically involved in receptor function and modulation. Front. Mol. Neurosci. *3*, 117.

Tomita, S. (2010). Regulation of ionotropic glutamate receptors by their auxiliary subunits. Physiology (Bethesda) *25*, 41–49.

Tomita, S., Chen, L., Kawasaki, Y., Petralia, R.S., Wenthold, R.J., Nicoll, R.A., and Bredt, D.S. (2003). Functional studies and distribution define a family of transmembrane AMPA receptor regulatory proteins. J. Cell Biol. *161*, 805–816.

Tomita, S., Adesnik, H., Sekiguchi, M., Zhang, W., Wada, K., Howe, J.R., Nicoll, R.A., and Bredt, D.S. (2005). Stargazin modulates AMPA receptor gating and trafficking by distinct domains. Nature *435*, 1052–1058.

Tomita, S., Sekiguchi, M., Wada, K., Nicoll, R.A., and Bredt, D.S. (2006). Stargazin controls the pharmacology of AMPA receptor potentiators. Proc. Natl. Acad. Sci. USA *103*, 10064–10067.

Traynelis, S.F., Wollmuth, L.P., McBain, C.J., Menniti, F.S., Vance, K.M., Ogden, K.K., Hansen, K.B., Yuan, H., Myers, S.J., and Dingledine, R. (2010). Glutamate receptor ion channels: structure, regulation, and function. Pharmacol. Rev. *62*, 405–496.

Turetsky, D., Garringer, E., and Patneau, D.K. (2005). Stargazin modulates native AMPA receptor functional properties by two distinct mechanisms. J. Neurosci. *25*, 7438–7448.

Twomey, E.C., Yelshanskaya, M.V., Grassucci, R.A., Frank, J., and Sobolevsky, A.I. (2016). Elucidation of AMPA receptor-stargazin complexes by cryo-electron microscopy. Science *353*, 83–86.

Wollmuth, L.P., Kuner, T., Jatzke, C., Seeburg, P.H., Heintz, N., and Zuo, J. (2000). The Lurcher mutation identifies delta 2 as an AMPA/kainate receptor-like channel that is potentiated by Ca(2+). J. Neurosci. *20*, 5973–5980.

Zachariassen, L.G., Katchan, L., Jensen, A.G., Pickering, D.S., Plested, A.J., and Kristensen, A.S. (2016). Structural rearrangement of the intracellular domains during AMPA receptor activation. Proc. Natl. Acad. Sci. USA *113*, E3950–E3959.

Zhao, Y., Chen, S., Yoshioka, C., Baconguis, I., and Gouaux, E. (2016). Architecture of fully occupied GluA2 AMPA receptor-TARP complex elucidated by cryo-EM. Nature *536*, 108–111.

## STAR★METHODS

### KEY RESOURCES TABLE

| REAGENT or RESOURCE | SOURCE | IDENTIFIER |
|---|---|---|
| Antibodies | | |
| Rabbit polyclonal C-terminal anti-GluA2/3 | Millipore | Cat#07-598; RRID: AB_11213931 |
| Rabbit polyclonal anti-TARP γ2 | Millipore | Cat#07-577; RRID: AB_310726 |
| Rat monoclonal anti-HA | Roche | Cat#11867423001; RRID: AB_390918 |
| Rabbit polyclonal anti-GFP | abcam | Cat#ab290l RRID: AB_303395 |
| Rabbit polyclonal anti-Actin | Sigma-Aldrich | Cat#A2066; RRID: AB_476693 |
| Peroxidase-conjugated AffiniPure Goat anti-Rabbit IgG | Jackson ImmunoResearch Labs | Cat#111-035-144; RRID: AB_2307391 |
| Peroxidase-conjugated AffiniPure Goat anti-Rat IgG | Jackson ImmunoResearch Labs | Cat#112-006-72; RRID: AB_11200672 |
| Chemicals, Peptides, and Recombinant Proteins | | |
| Glutamate | Sigma-Aldrich | Cat# G2834; CAS: 6106-04-3 |
| Kainate | Sigma-Aldrich | Cat#K2389; CAS: 58002-62-3 |
| 1-Naphthylacetyl spermine | Sigma-Aldrich | Cat#N193; |
| Cyclothiazide | Sigma-Aldrich | Cat#C9847; CAS: 2259-96-3 |
| Concanavalin A | Sigma-Aldrich | Cat#C2010; CAS: 11028-71-0 |
| Collagenase | Sigma-Aldrich | Cat#C9891; CAS: 9001-12-1 |
| Lipofectamine® 2000 | Thermo Fisher Scientific | Cat#11668027 |
| Poly-D-lysine hydrobromide | Sigma-Aldrich | Cat#P0899; CAS: 27964-99-4 |
| Protein A-agarose beads | Calbiochem | Cat#IP06 |
| EZ-Link HPDP-Biotin | Thermo Fisher Scientific | Cat#21341 |
| Streptavidin- Sepharose | Pierce | Cat#20353 |
| Critical Commercial Assays | | |
| Q5-Site-Directed Mutagenesis Kit | New England Biolabs | Cat#E0554S |
| AmpliCap-Max T7 High Yield Message Maker Kit | CellScript | Cat#C-ACM04037 |
| AmpliCap SP6 High Yield Message Maker Kit | CellScript | Cat#C-AC0706 |
| EZ-ECL Kit | Biological Industries | Cat#20-500-120 |
| Deposited Data | | |
| Structure of GluA2 tetramer | Sobolevsky et al., 2009 | PDB: 3KG2 |
| Experimental Models: Cell Lines | | |
| Human Embryonic Kidney (HEK) 293 cells | ATCC | Cat#CRL-1573 |
| Experimental Models: Organisms/Strains | | |
| *Xenopus laevis* frogs | Xenopus1 | http://www.xenopus1.com/ |
| Recombinant DNA | | |
| Plasmid: pGEM-HE GluA3 chimeras, Table S1 | Ayalon and Stern-Bach, 2001 | N/A |
| Plasmid: pRK A3(K2/M1-3,M4-CT) | This paper | N/A |
| Plasmid: pRK HA-tagged GluK2 | Priel et al., 2006 | N/A |
| Plasmid: pRK HA-tagged GluK2 chimeras, Table S2 | This paper | N/A |
| Plasmid: pRK HA-tagged GluA2 | This paper | N/A |
| Plasmid: pRK EGFP-tagged TARP γ2 | Priel et al., 2005 | N/A |
| Plasmid: pGEM-HE EGFP-tagged TARP γ2 | This paper | N/A |
| Plasmid: pGEM-HE EGFP-tagged TARP γ8 | This paper | N/A |
| Plasmid: pGEM-HE EGFP-tagged TARP γ3 | Gift of E. Isacoff (Hastie et al., 2013) | N/A |
| Plasmid: pGEM-HE EGFP-tagged TARP γ4 | Gift of E. Isacoff (Hastie et al., 2013) | N/A |

(*Continued on next page*)

*Continued*

| REAGENT or RESOURCE | SOURCE | IDENTIFIER |
|---|---|---|
| Plasmid: pGEM-HE EGFP-tagged TARP γ2/γ8 chimeras, Figure 6 | This paper | N/A |
| Software and Algorithms | | |
| pCLAMP8.2 | Molecular Devices | N/A |
| pCLAMP10 | Molecular Devices | N/A |
| ClampFit10.2 | Molecular Devices | N/A |
| Origin 8 | OriginLab | http://www.originlab.com/ |
| Quantity One | Bio-Rad Laboratories | http://www.bio-rad.com/en-us/product/quantity-one-1-d-analysis-software |
| ImageJ | Schneider et al., 2012 | https://imagej.nih.gov/ij/ |
| Clone Manager Professional 9 | Scientific & Educational Software | http://www.scied.com/pr_cmpro.htm |
| PyMOL | Molecular Graphics System, Version 1.74; Schrodinger, LLC | https://www.pymol.org |

## CONTACT FOR REAGENT AND RESOURCE SHARING

Further information and requests for resources and reagents should be directed to and will be fulfilled by the Lead Contact, Yael Stern-Bach (yaelste@ekmd.huji.ac.il).

## EXPERIMENTAL MODEL AND SUBJECT DETAILS

### *Xenopus laevis* Frogs

*Xenopus laevis* frogs (females, age 1-3 years old) were used as a source for oocytes for heterologous expression and whole-cell two-electrode voltage clamp (TEVC) recordings. Maintenance of the frogs and extraction of oocytes were performed in accordance with the National Institutes of Health guidelines for the Care and Use of Laboratory Animals and the Israeli law for animal experimentation and were approved by the Institutional Animal Care and Use Committee (IACUC) of the Hebrew University of Jerusalem.

### Cultured Cells

Human Embryonic Kidney 293 (HEK293) cells were used for heterologous expression and patch-clamp electrophysiology. Cells were obtained from ATCC and were not further authenticated. Cells were grown and maintained using standard protocols at 37°C with 5% CO2. Cells were passed twice a week and were used until the 20th pass.

## METHOD DETAILS

### Molecular Biology

AMPAR GluA1, GluA2 and GluA3, used in this study or served as templates for the various chimeras, were Q- and flip-forms and the KAR GluK2 was QVC-form. The GluA3 chimeras used in this study were described previously and were inserted in pGEM-HE (Ayalon and Stern-Bach, 2001). Chimera A3(K2/M1-3,M4-CT) was subcloned in pRK for patch-clamp analysis in HEK293 cells. Part of the GluK2 chimeras were described previously (Ayalon and Stern-Bach, 2001) and others were generated by a similar strategy using overlap PCR extension. For this study, all GluK2 chimeras were inserted in pRK and tagged with a HA epitope at the N-terminal domain after the leader peptide, similar to intact GluK2 (Priel et al., 2006). Similarly, GluA2 was tagged with HA after the leader peptide and inserted in pRK. All TARP isoforms and chimeras carried an EGFP tag at the C-terminal domain. EGFP-tagged γ8 was constructed similar to γ2 (Priel et al., 2005) and EGFP-tagged γ3 and γ4 were a gift from Ehud Isacoff (Hastie et al., 2013). EGFP-tagged γ2/γ8 chimeras were constructed by PCR using the Q5-DNA polymerase Site-Directed Mutagenesis Kit (New England Biolabs). All TARP isoforms and chimeras were in pGEM-HE. For patch-clamp analysis in HEK293 cells we used EGFP-tagged γ2 in pRK (Priel et al., 2005). Receptor and TARP chimera boundaries are specified in Figure 7A and 7B, respectively. For expression in oocytes cRNA was transcribed from pGEM-HE or pRK plasmids using AmpliCap-Max T7 High Yield Message Maker Kit or AmpliCap SP6 High Yield Message Maker Kit (CellScript), respectively, and pRK plasmids were used for expression in HEK293 cell.

### Heterologous Expression and Electrophysiology

For expression in *Xenopus laevis* oocytes, stage V-VI oocytes were prepared and injected with cRNA as previously described (Ayalon and Stern-Bach, 2001). Oocytes were obtained in lobes from an anesthetized frog through a small abdominal incision, harvested and treated for 1-2 hr with Collagenase (Sigma-Aldrich) in calcium-free buffered solution to remove connective tissue and capillaries, and

incubated at 17°C in buffered solution containing sodium pyruvate, 10,000 units/l penicillin, 10mg/l streptomycin, and 50 mg/l gentamycin. Oocytes were injected up to 24 hr after preparation and were assayed 1-3 days later. Injected oocytes were kept at a controlled environment of 17°C. Receptor and TARP constructs were usually injected at 1:1 amounts (1-3 ng cRNA/oocyte) (Priel et al., 2005) and protein expression levels were routinely monitored by Western-blot analysis. Whole-cell two electrode voltage clamp (TEVC) recordings were performed 2-3 days post injection at 17°C, at holding potential of −70mV, using GeneClamp500 connected to Digidata 1322A and pCLAMP8.2 (Molecular Devices) as previously done (Ayalon and Stern-Bach, 2001). Electrodes were filled with 3 M KCl and had resistance of 0.5–1 MΩ. Oocytes were continuously perfused with normal frog ringer (NFR) solution containing (in mM): 10 HEPES, pH 7.4, 115 NaCl, 2.5 KCl, 1.8 $CaCl_2$, and 0.1 $MgCl_2$. To block receptor desensitization, cyclothiazide (0.1mM) (Sigma-Aldrich) was applied with the agonists glutamate or kainate (Sigma-Aldrich) for intact AMPARs and GluA3 chimeras, and for intact GluK2 and GluK2 chimeras the oocytes were treated with 1mg/ml Concanavaline A (Sigma-Aldrich) for 5 min prior to agonist application. 1-Naphthylacetyl spermine (Sigma-Aldrich) was used to block leak currents. Current-Voltage curves were obtained by applying 1 s voltage ramps (from −70 to +70mV) on plateau response to glutamate in the presence of cyclothiazide. Currents (after subtraction of the basal response before glutamate application) were normalized to the value obtained at −70mV, and the rectification index (R.I.) was calculated as the ratio between the conductance at +70mV and −70mV. Dose-response curves for glutamate were constructed by applying consecutive increasing concentrations of glutamate to individual oocytes and current responses were normalized to the maximum response. Data was analyzed using ClampFit10.2 (Molecular Devices) and Origin 8 (OriginLab) software. All experiments were repeated in oocytes obtained from at least 3 independent frogs (separated in time) and the total number of recorded oocytes is indicated in the respective figure and table legends. The experiments were not randomized, but oocytes expressing a particular construct were randomly selected for recordings. Group sample sizes were chosen based on previous studies (e.g., Stern-Bach et al., 1994; Ayalon and Stern-Bach, 2001; Priel et al., 2005) and no statistical methods were used to predetermine sample size. The investigators were not blinded to allocation during experiments and outcome assessment. No outliers were excluded from analysis. Statistical differences between groups were examined by One Way ANOVA (ORIGIN 8 software).

For expression in HEK293 cells, cells were grown and maintained using standard protocols and transfected using Lipofectamine 2000 (Thermo Fisher Scientific) as done previously (Priel et al., 2005; Priel et al., 2006). Cells used for electrophysiology were re-plated 24 hr after transfection on coverslips coated with Poly-D-lysine hydrobromide (0.1mg/ml) (Sigma-Aldrich) and 36-48 hr later subjected to fast-flow outside-out patch clamp recordings as done before (Priel et al., 2005; Priel et al., 2006). Currents were recorded using Axopatch 200B connected to Digidata 1322A and pCLAMP10 (Molecular Devices) and analyzed using ClampFit10.2 and Origin 8. Sampling frequency was set to 10 kHz, and the low-pass filter was set to 2 kHz. Patch electrodes were fabricated from borosilicate glass with a resistance of 2–4 MΩ. The extracellular solution contained (in mM): 150 NaCl, 2.8 KCl, 0.5 $MgCl_2$, 2 $CaCl_2$, 10 HEPES, adjusted to pH 7.4 with NaOH. The pipette solution contained (in mM): 110 CsF, 30 CsCl, 4 NaCl, 0.5 $CaCl_2$, 10 EGTA, 10 HEPES, adjusted to pH 7.2 with CsOH. For the rapid application of agonists, solutions were applied from a double-barrel glass (theta tube) mounted on a piezoelectric translator (Burleigh, Fishers, NY). We estimated the speed of solution exchange by recording the open tip potentials with solutions of different ionic strengths after expelling the patch from the electrode. The 10%–90% solution exchange was typically < 500 μs. Receptor desensitization was measured by applying agonists for 500ms, and the desensitization rate (τdes) was estimated by a single exponential fitting of the current decay starting from 95% of the peak to the baseline current. Deactivation rates were measured similarly for currents evoked by 1ms agonist application. All experiments were repeated in cells obtained from at least 3 independent transfections (separated in time) and the total number of recorded outside-out patches is indicated in the respective figure and table legends. The experiments were not randomized, but cells expressing a particular construct were randomly selected for patch-clamping. Group sample sizes were chosen based on previous studies (Priel et al., 2005; Priel et al., 2006) and no statistical methods were used to predetermine sample size. The investigators were not blinded to allocation during experiments and outcome assessment. Recordings less than 20pA were excluded from the analysis. Statistical differences between groups were examined by One Way ANOVA (ORIGIN 8 software).

## Biochemical Assays

Cell surface biotinylation assays on oocytes and HEK293 cells expressing the various constructs were done as previously (Ayalon and Stern-Bach, 2001; Priel et al., 2005). For oocyte biotinylation, 20 oocytes expressing a particular construct were incubated with 0.5 mg/ml EZ-Link HPDP-Biotin (Thermo Fisher Scientific) in NFR for 30 min at 17°C. Oocytes were washed 5 times with NFR and homogenized through a p200 pipette tip in Buffer H containing 100 mM NaCl, 20 mM Tris-Cl, pH 7.4, 1% Triton X-100, and protease inhibitor cocktail in a volume of 40 μL per oocyte. Lysates were centrifuged at 14,000 × g for 5 min. Cleared lysate (50 μl) was reserved as the total protein sample (T). The remaining lysate was incubated with 50 μL of 50% Streptavidin-Sepharose slurry (Pierce) for 3 hr at 4°C. Beads were washed five times in Buffer H, and surface biotinylated proteins (S) were eluted by 5 min boiling in SDS-PAGE sample buffer. For HEK293 cells, transfected cells grown in poly-d-lysine-coated 25 $cm^2$ culture dishes were washed three times with ice-cold PBS supplemented with 1.0 mM $MgCl_2$ and 0.5 mM $CaCl_2$ (PBSCM) and incubated for 15 min with 0.5 mg/ml EZ-Link HPDP-Biotin (Thermo Fisher Scientific) in cold PBSCM, pH 8.0, with gentle agitation at 4°C. Cells were washed once and incubated for 10 min with a quenching buffer 192 mM glycine and 25 mM Tris in PBSCM). Cells were then rinsed twice in cold PBS, collected, homogenized in lysis buffer (1% Triton X-100, 20 mM HEPES, pH 7.4, and 150 mM NaCl), and centrifuged. Supernatants were incubated with 50 μL of 50% slurry of Streptavidin-Sepharose (Pierce) overnight at 4°C, washed three times with lysis buffer and surface biotinylated proteins (S) were eluted by 5 min boiling in SDS-PAGE sample buffer.

For the co-immunoprecipitation assays in HEK293 cells, 36 hr post transfection cells grown in 6-well plates were rinsed once in PBS, collected and homogenized in 100μl homogenization buffer as done previously (Priel et al., 2005). The majority of the fraction (80μl) was incubated for 2 hr with 3μg rabbit polyclonal anti-TARP γ2 antibodies (Millipore) at 4°C, with gentle agitation, while the remaining fraction was kept for Western-blot analysis as total (T). Antibody supplemented homogenates were incubated overnight with 50μl of pre-washed Protein A-agarose beads (Calbiochem) at 4°C, with gentle agitation. Beads were washed three times with cold PBS and centrifuged in 14000 g for 5 min at 4°C and immunoprecipitated bound proteins (IP) were eluted were eluted by 10 min boiling in SDS-PAGE sample buffer.

In both assays (biotinylation and co-immunoprecipitation) 5% of the total protein homogenate loaded on the respective separating beads and 50% of the eluted fraction were subjected to SDS-PAGE and Western-blot analysis. For detection the following primary antibodies were used: Rabbit polyclonal C-terminal anti-GluA2/3 at 1:2000 dilution (Millipore), rabbit polyclonal anti-TARP γ2 at 1:2000 dilution (Millipore), rat monoclonal anti-HA at 1:500 dilution (Roche), rabbit polyclonal anti-Actin at 1:1000 dilution (Sigma-Aldrich) and rabbit polyclonal anti-GFP at 1:5000 dilution (abcam). The appropriate Peroxidase-conjugated AffiniPure Goat anti-Rabbit IgG and Goat anti-Rat IgG secondary antibodies were from Jackson ImmunoResearch Labs. The reacting bands were visualized by the chemiluminescence EZ-ECL Kit (Biological Industries) using the ChemiDoc XRS system (Bio-Rad Laboratories). Densitometry analysis was done using the Quantity One software (Bio-Rad Laboratories) or ImageJ (Schneider et al., 2012).

The biotinylation and co-immunoprecipitation experiments were repeated at least 3 times as indicated in the respective figure and table legend. Group sample sizes were chosen based on previous studies (e.g., Stern-Bach et al., 1994; Ayalon and Stern-Bach, 2001; Priel et al., 2005). The investigators were not blinded to allocation during experiments and outcome assessment. No outliers were excluded from analysis. Statistical differences between groups were examined by One Way ANOVA (ORIGIN 8 software).

## QUANTIFICATION AND STATISTICAL ANALYSIS

Data are presented as mean ± standard error of the mean (SEM). Number of samples (n) refers to the total number of recorded oocytes or outside-out patches of HEK293 cells (collected from at least 3 independent injections or transfections, respectively) or to the number of biotinylation and co-immunoprecipitation assays as indicated in the figure and table legends. Statistical differences between groups were examined by One Way ANOVA using the ORIGIN 8 software (OriginLab) and all datasets displayed normal distribution; no other statistical analysis was used. P values less than 0.05 were considered statistically significant: (*) $p < 0.05$, (**) $p < 0.01$, (***) $p < 0.001$.